Journal for ImmunoTherapy of Cancer

PKR induces TGF-β and limits oncolytic immune therapy

Bangxing Hong,[1] Upasana Sahu,[1] Matthew P Mullarkey,[1] Evan Hong,[1] Guangsheng Pei,[2] Yuanqing Yan,[1] Yoshihiro Otani,[1] Yeshavanth Banasavadi-Siddegowda,[1] Huihui Fan,[2] Zhongming Zhao ,[2] Jianhua Yu,[3] Michael A Caligiuri,[3] Balveen Kaur [1]

To cite: Hong B, Sahu U, Mullarkey MP, *et al*. PKR induces TGF-β and limits oncolytic immune therapy. *Journal for ImmunoTherapy of Cancer* 2023;**11**:e006164. doi:10.1136/jitc-2022-006164

► Additional supplemental material is published online only. To view, please visit the journal online (http://dx.doi.org/10.1136/jitc-2022-006164).

Accepted 23 January 2023

[1]Department of Neurosurgery, McGovern Medical School, The University of Texas Health Science Center at Houston, Houston, Texas, USA
[2]Center for Precision Health, School of Biomedical Informatics, The University of Texas Health Science Center at Houston, Houston, Texas, USA
[3]Department of Immuno-Oncology, City of Hope National Medical Center, Duarte, California, USA

Correspondence to
Professor Balveen Kaur; bkaur@augusta.edu

Dr. Bangxing Hong; bhong@augusta.edu

ABSTRACT

Background Mammalian cells have developed multiple intracellular mechanisms to defend against viral infections. These include RNA-activated protein kinase (PKR), cyclic GMP-AMP synthase and stimulation of interferon genes (cGAS-STING) and toll-like receptor-myeloid differentiation primary response 88 (TLR-MyD88). Among these, we identified that PKR presents the most formidable barrier to oncolytic herpes simplex virus (oHSV) replication in vitro.

Methods To elucidate the impact of PKR on host responses to oncolytic therapy, we generated a novel oncolytic virus (oHSV-shPKR) which disables tumor intrinsic PKR signaling in infected tumor cells.

Results As anticipated, oHSV-shPKR resulted in suppression of innate antiviral immunity and improves virus spread and tumor cell lysis both in vitro and in vivo. Single cell RNA sequencing combined with cell-cell communication analysis uncovered a strong correlation between PKR activation and transforming growth factor beta (TGF-ß) immune suppressive signaling in both human and preclinical models. Using a murine PKR targeting oHSV, we found that in immune-competent mice this virus could rewire the tumor immune microenvironment to increase the activation of antigen presentation and enhance tumor antigen-specific CD8 T cell expansion and activity. Further, a single intratumoral injection of oHSV-shPKR significantly improved the survival of mice bearing orthotopic glioblastoma. To our knowledge, this is the first report to identify dual and opposing roles of PKR wherein PKR activates antivirus innate immunity and induces TGF-ß signaling to inhibit antitumor adaptive immune responses.

Conclusions Thus, PKR represents the Achilles heel of oHSV therapy, restricting both viral replication and antitumor immunity, and an oncolytic virus that can target this pathway significantly improves response to virotherapy.

WHAT IS ALREADY KNOWN ON THIS TOPIC

⇒ RNA-activated protein kinase (PKR) is known to be a molecular sensor for intracellular pathogens.
⇒ Upon sensing RNA in the cytosol, it orchestrates a defense response to initiate innate immunity.

WHAT THIS STUDY ADDS

⇒ This is the first study, in our knowledge, to show that PKR also activates immune suppressive TGF-β signaling which can regulate immune responses.

HOW THIS STUDY MIGHT AFFECT RESEARCH, PRACTICE OR POLICY

⇒ We have identified two dual and opposing roles of PKR wherein PKR activates antivirus innate immunity and blocks antitumor adaptive immunity.
⇒ This provides a unique opportunity to maximizing antitumor effects by biological drugs that are heavily regulated by PKR.

INTRODUCTION

Viral infection is sensed and cleared through multiple host intracellular antiviral mechanisms which includes activation of RNA-activated protein kinase (PKR),[1–3] cyclic GMP-AMP synthase and stimulation of interferon genes (cGAS-STING),[4–7] and toll-like receptor-myeloid differentiation primary response 88 (TLR-MyD88)[8 9] signaling. Malignant cells have compromised antiviral responses[10] which complement the defects of attenuated oncolytic viruses, permitting viral replication and resulting in cancer cell destruction.[11] Although oncolytic viruses can infect and replicate in tumor cells, multiple tumor intrinsic and extrinsic factors, including interferon signaling,[12] growth factors,[13] and tumor cell heterogeneity,[14] limit the efficacy of oncolytic viral therapy.[10 15] Additionally, recent studies have also uncovered that many tumors, including glioblastoma (GBM), have an inherent resistance to oncolytic virus therapy.[16–18] Thus, there is an urgent need to better understand the inherent antiviral host response in both malignant and non-malignant cells in order to enhance the likelihood of a successful antitumor response using oncolytic virus therapy.

PKR presents a formidable cellular barrier for viral infections, but its impact on cancer growth and progression is not clear. While PKR activation in cancer cells has been shown to activate tumor cell death in untreated cancer cells,[19] its activation is also associated with glioma cell stemness and resistance

to chemotherapy.[20] Apart from direct virus clearance, PKR-induced inflammatory responses are also thought to reduce T cell activity and increased Treg functionality.[21] Since oncolytic virus therapy depends on both virus-induced lytic tumor cell death and the ensuing activation of antitumor immunity, we created an oncolytic virus oHSV-shPKR that can knock out infected cell PKR. While this virus could increase herpes simplex virus (HSV) spread in both resistant and sensitive cancer cells, we observed that this virus could also induce antigen-specific T-cell expansion and enhanced antitumor immunity. Mechanistically, we discovered that PKR signaling positively regulates immunosuppressive TGF-β in the tumor microenvironment and that modulation of PKR reduces TGF-β activation, effectively releasing the immunosuppressive brakes and allowing for better antitumor immunity.

Our results suggest that while PKR orchestrates innate antiviral signaling, it also educates an immune-suppressive environment in the tumor. These observations provide significant insight into the tumor cell and tumor microenvironment and translationally set the stage for next-generation oncolytic viruses which can be built on this platform with the end goal of achieving increased virus replication and enhanced antitumor immunity.

RESULTS

oHSV-shPKR enhances oncolytic killing in vitro and in vivo

To evaluate possible resistance mechanisms to oHSV, we first evaluated relative sensitivity to oncolytic herpes simplex virus (oHSV) in a panel of glioma cell lines and primary patient-derived neurosphere cultures. Evaluation of infected cell spread revealed that while the virus could efficiently infect, replicate and spread over time in sensitive cells, some glioma cells had an inherent resistance to oHSV replication in vitro (online supplemental figure 1a,b). To examine the effect of known virus clearance signaling pathways on oHSV resistance, we used siRNA to singly knock down expression of either cGAS-STING or PKR, or used an inhibitor against TLR-Myd88 in LN229, resistant glioma cells and found that PKR blockade significantly and robustly sensitized resistant glioma cells to oHSV (figure 1A, online supplemental figure 2a,b, online supplemental table 1). Apart from resistant glioma cells, PKR knock down also further sensitized U87 (oHSV sensitive) cells to oHSV infection and killing (online supplemental figure 2c-e). In order to further investigate the role of PKR in oHSV therapy, we created an oHSV that expresses human PKR targeting shRNA under a H1 promotor (oHSV-shPKR) and a control virus that encodes for a scrambled control shRNA (oHSV-shCtl) (online supplemental figure 3). Western blot analysis of GSC20 (oHSV resistant) cells treated with oHSV-shPKR or oHSV-shCtl confirmed the reduction in cellular PKR on treatment (figure 1B). RNA sequencing and gene set enrichment analysis (GSEA) of sensitive (U251) and resistant (GSC20) glioma cells showed a significant negative enrichment in antiviral signaling of oHSV-shPKR-treated cells (figure 1C). Quantification of virus replication measured in real time by live cell fluorescent microscopy (for GFP+ve infected cells) revealed an increase in both sensitive (GBM12) and resistant (GSC20) human glioma cells (figure 1D). Flow cytometry analysis to evaluate live dead cells also showed a significant increase in tumor cell death on treatment with oHSV-shPKR relative to HSVQ in both sensitive (GBM12 and LN229) and resistant (GSC20 and GBM28) human glioma cells (figure 1E and online supplemental figure 4a,b).

Next, we evaluated the impact of PKR silencing on oHSV therapy of human brain tumors in mice. Mice bearing established intracranial human tumors were treated with either oHSV-shPKR or oHSV-shCtl and monitored for survival. Results show that tumor-bearing mice treated with oHSV-shPKR had a significant therapeutic advantage compared with mice treated with control virus in both HSV-sensitive (GBM12) and HSV-resistant (GBC20) glioma tumor models in mice (figure 1F–G). Immunofluorescence staining of tumor sections derived from GBM12 tumor-bearing mice treated with oHSV-shCtl or oHSV-shPKR revealed increased tumor cell death (cleaved caspase 3) and increased virus (ICP4) in tumor tissue 8 days after treatment (figure 1H).

oHSV-shPKR increases dendritic cell and T cell activation

Apart from immediate tumor cell lysis, a large part of the therapeutic benefit of oncolytic virus therapy is attributed to its ability to induce antitumor immunity. However, it has not been clear whether innate defense responses that modulate virus replication and hence oncolytic death (death induced by direct virus replication) can interact and/or regulate antitumor adaptive immunity.

To examine this, we co-cultured peripheral blood mononuclear cells (PBMCs) with oHSV-sensitive GBM12 and resistant GSC20 glioma cells infected with oHSV-shCtl (multiplicity of infection (MOI)=0.02). In the absence of PBMCs, sensitive (GBM12) cells showed efficient tumor cell death on infection (figure 2A). Tumor cell death of sensitive GBM12 cells was not changed with PBMC overlay (GBM12, figure 2A). On the otherhand, resistant glioma cells (GSC20, MOI=0.02) showed no significant tumor cell death with viral infection alone. PBMC co-culture of these infected GSC20 cells showed increased susceptibility to immune cell-mediated killing (figure 2B). Similar results were seen with LN229 and GBM28 cells (online supplemental figure 5a,b). Together, these results imply that the primary mechanism of cell death in oHSV-sensitive cells is virus-mediated lytic destruction, while in resistant cells the primary mechanism of cell death is due to the immune cell-mediated killing.

Since PKR modulation sensitized resistant cells to virotherapy, we evaluated the impact of oHSV-shPKR treatment on PBMC-mediated killing of sensitive (GBM12, MOI=0.002, figure 2C,D) and resistant (GSC20, MOI=0.02, figure 2E,F) cells. As anticipated, without PBMC co-culture, oHSV-shPKR treatment increased the

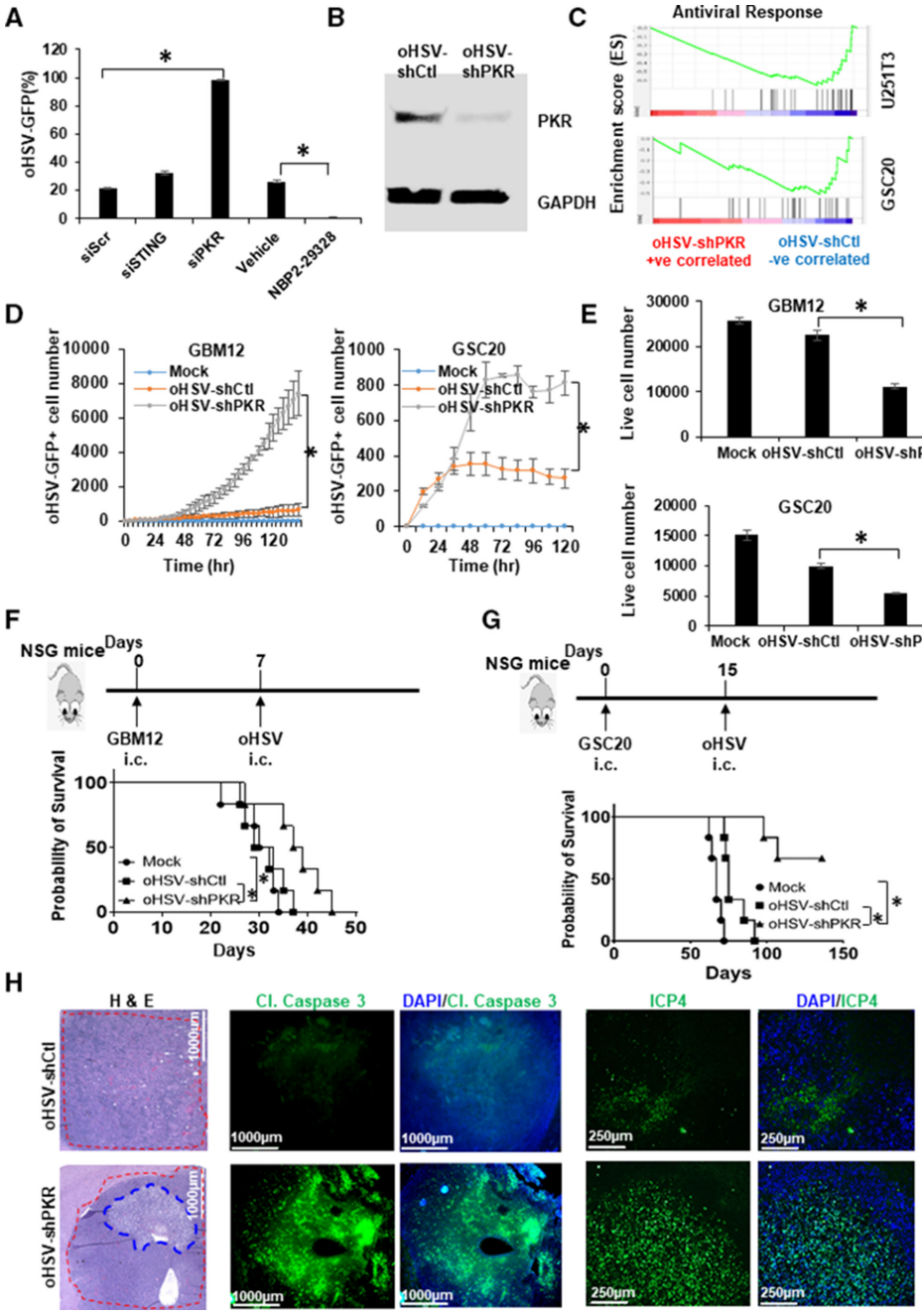

Figure 1 RNA-activated protein kinase (PKR) signaling controls oncolytic HSV (oHSV) sensitivity in glioblastoma (GBM). (A) LN229 (oHSV resistant) cells were transfected with scrambled (Scr) control, STING, or PKR siRNA, or treated with a MyD88 inhibitor (NBP2-29328, 5 μM) for 16 hours and then infected with oHSV-GFP for another 72 hours at multiplicity of infection (MOI)=0.02. oHSV-infected LN229 cells were analyzed for GFP+ve infected cells using flow cytometry (n=3/g). (B) Representative western blots of resistant GSC20 cells treated with oHSV-shCtl or oHSV-shPKR at MOI=0.02 for 72 hours. (C) mRNA-seq analysis of resistant (GSC20) and sensitive (U251T3) cells infected with oHSV-shCtl and oHSV-shPKR. Gene set enrichment analysis of Gene Ontology pathways related to antiviral response. (D) Sensitive (GBM12) and resistant (GSC20) cells were infected with oHSV-shCtl or oHSV-shPKR at MOIs (0.1 or 0.02 for GBM12 and GSC20, respectively). Quantification of mean GFP^{+ve}cells±SD over time by live cell fluorescent imaging (n=3/g). (E) Quantification of live tumor cells post-oHSV infection in sensitive (GBM12) and resistant (GSC20) cells was performed using aqua live/dead staining and quantified by flow cytometry (mean±SD for n=3 g). (F–G) Anti-glioma efficacy of oHSV-shPKR. NOD scid gamma (NSG) mice implanted with $2e^5$ of sensitive (GBM12, F) or $5e^5$ of resistant (GSC20, G) cells were treated with $5e^4$ p.f.u. oHSV-shPKR or oHSV-shCtl and monitored for survival (n=10/group). (H) GBM12 tumors were established in mice as in (F). Mice were sacrificed on day 15 post-tumor implantation and tumor-bearing brain hemispheres were analyzed for tumor cell lysis by H&E staining and cleaved caspase-3 immunofluorescence, and oHSV infection by ICP4 immunofluorescence. Nuclei were counterstained with 4'6-diamidino-2-phenylindole (DAPI). Representative results from one of three mice were shown. For H&E staining, red dashed line represents tumor area, while blue dashed line represents necrosis and oHSV infection area. All experiments were repeated three times in triplicate independently. Error bars are SD, Student's t-test (*p value <0.05).

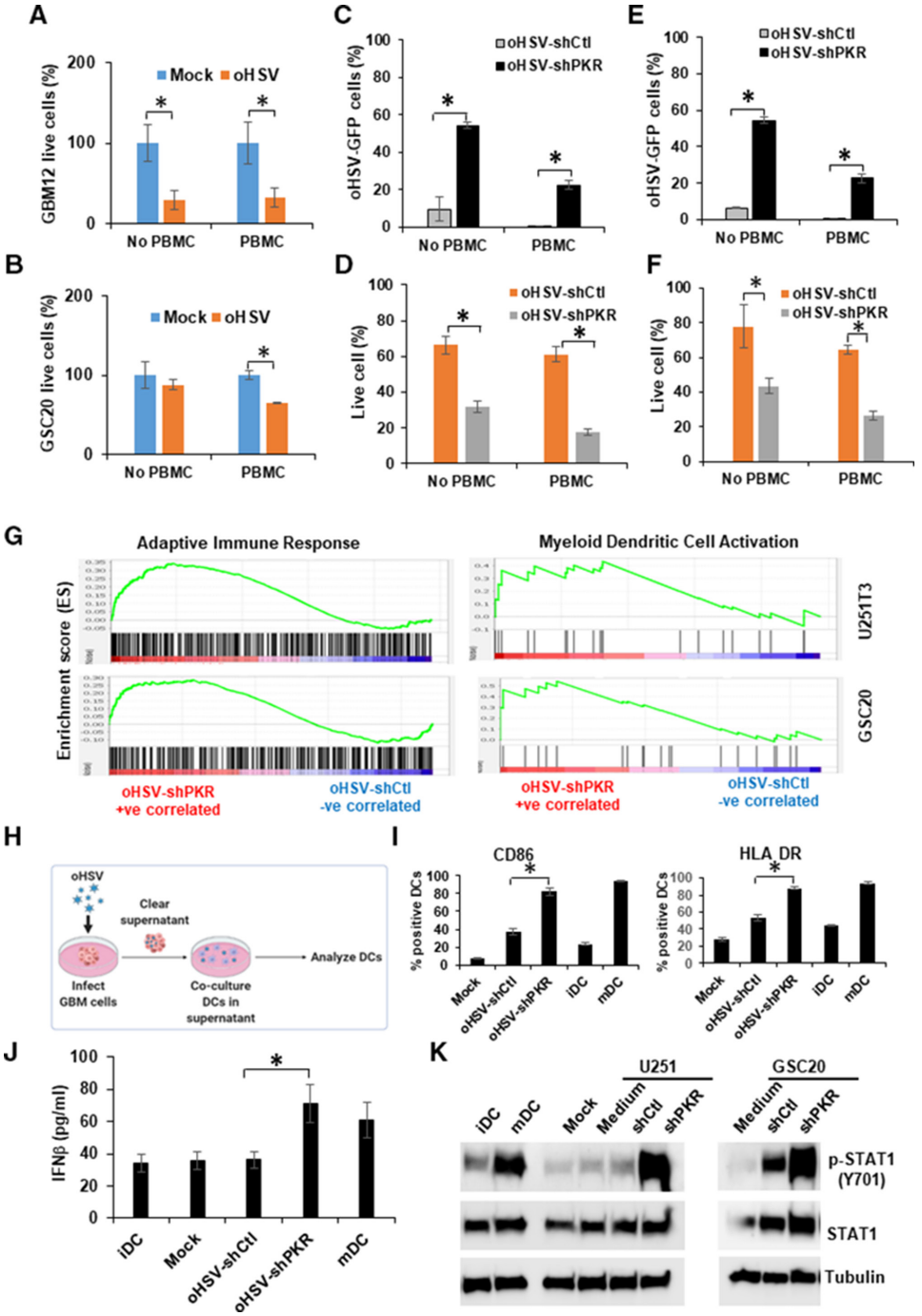

Figure 2 oHSV-shPKR induces immune cell killing and dendritic cell activation. (A, B) oncolytic herpes simplex virus (oHSV)-sensitive GBM12 (A) and oHSV-resistant GSC20 (B) cells were infected with oncolytic herpes simplex virus expressing green fluorescent protein (oHSV-GFP) (oHSV) at multiplicity of infection (MOI)=0.02, in the presence or absence of human peripheral blood mononuclear cells (PBMCs) (E:T=1:5) for 96 hours. Tumor cell lysis was quantified using aqua live/dead staining (n=3). (C–F) GBM12 (C, D) or GSC20 (E, F) cells were infected with oHSV-shCtl or oncolytic herpes simplex virus expressing human PKR shRNA (oHSV-shPKR) for 24 hours (MOI=0.002 for GBM12, or MOI=0.02 for GSC20) and then co-cultured in the presence or absence of human PBMCs (1:5) for 96 hours. oHSV infection (C, E) by fluorescent imaging and tumor cells lysis (D, F) by aqua live/dead staining was quantified. Data shown are mean±SD (n=3/g). (G) mRNA-seq analysis of U251T3 and GSC20 cells infected with oHSV-shCtl and oHSV-shPKR. Gene set enrichment analysis of Gene Ontology pathways related to antiviral response, adaptive immune response, and myeloid dendritic cell (DC) activation. (H) Diagram of experimental setup co-culturing PBMC-derived DCs with supernatants from GSC20 cells infected with either oHSV-shPKR or oHSV-shCtl. (I) DC activation was analyzed by cell surface CD86 and human leukocyte antigen (HLA) DR expression on $CD1a^{+ve}$ DCs using flow cytometry (n=3). iDC, immature dendritic cell; mDC, LPS matured dendritic cell. (J) Interferon-β (IFNβ) secretion from DCs co-cultured with supernatant from oHSV-shPKR or oHSV-shCtl-infected GSC20 cells was analyzed by ELISA (n=3). (K) STAT1 activation in DCs co-cultured with supernatant from oHSV-shPKR or oHSV-shCtl-infected GSC20 cells was analyzed by western blotting. Data represent three independent experiments in triplicate. Error bars are SD, Student's t-test (*p value <0.05).

% of infected cells relative to oHSV-shCtl treated cells in both sensitive and resistant cells (figure 2C,E). Co-culture with PBMC reduced the number of infected cells in both sensitive (GBM12, figure 2C) and resistant (GSC20, figure 2E) glioma cells. Quantification of live-dead cells revealed that oHSV-shPKR sensitized both sensitive and resistant GBM cells to killing in both the presence and absence of PBMC (figure 2D–F). Thus, oHSV-shPKR infection sensitized both sensitive and resistant tumor cells to virus as well as immune cell-mediated killing.

Since about 45%–70% of human PBMCs are constituted of T cells, we rationalized that this was likely due to enhanced T cell activation and T cell-mediated killing. To evaluate the mechanism by which oHSV-shPKR could affect immune cell activation, we compared total mRNA-seq of resistant GSC20 and sensitive cells U251T3 infected with oHSV-shCtl or oHSV-shPKR. GSEA showed that oHSV-shPKR infection resulted in an enrichment of signaling pathways relevant to adaptive immunity, including activation of antigen presenting dendritic cells (DCs) (figure 2G). To measure changes in cytotoxic T cell activation in the PBMCs overlaid on treated glioma cells, we measured changes in CD69 activation and interferon-γ (IFNγ) release in the conditioned medium of infected glioma cells co-cultured with PBMC. A significant increase in CD69+CD8+ (%) T cells (online supplemental figure 6a) and IFNγ secretion in conditioned medium of PBMC cultured with oHSV-shPKR relative to oHSV-shCtl infected cells (online supplemental figure 6b) suggested improved T cell activation.

Since DCs play a key role in the activation of T cells, we evaluated the effect of oHSV-shPKR infected tumor cell lysates on antigen presentation. To test this, we infected GSC20 cells with oHSV-shPKR or control virus for 48 hours and then incubated human PBMC-derived DCs with culture supernatants for 48 hours (figure 2H). Analysis of cell surface expression of HLA-DR and CD86 on $CD1a^+$ DCs revealed a significant increase in DC activation when cultured in the presence of supernatant from oHSV-shPKR-infected cells compared with control (figure 2I and online supplemental figure 7). Additionally, DCs incubated with oHSV-shPKR supernatant had a significant increase in interferon-beta (IFN-β) secretion (figure 2J), as well as a significant increase in STAT-1 signaling, as measured by phosphorylated STAT-1 via western blot analysis (figure 2K). Immature (iDC) and mature dendritic cells (mDCs) were used as negative and positive controls in the assays. Importantly, we did not detect an effect of oHSV-shPKR infected supernatant on DC apoptosis (online supplemental figure 7). Thus, oHSV-shPKR infection dramatically increases antigen presentation and DC activation in the tumor microenvironment.

DCs present antigens to T cells to induce antitumor immune response. Thus, we evaluated changes in T cell activation. RNA-seq data from GSC20 and U251T3 cells treated with oHSV-shPKR or control virus revealed an enrichment of signaling pathways related to T and B cell activation (figure 3A,B). To scrutinize the impact of oHSV-shPKR on the generation of antigen-specific cytotoxic T lymphocytes (CTLs), we incubated human T cells with DCs (precharged with infected glioma cell lysates) and examined the effect on T cell immunomodulatory activity (figure 3C shows the experimental schema). Flow cytometry analysis of T cells incubated with DCs charged with oHSV-shPKR revealed an increase in CD69 expression on both $CD8^+$ and $CD4^+$ T cells (figure 3D, online supplemental figure 8a) and intracellular staining for effector molecules IFN-γ and tumor necrosis factor alpha (TNF-α) relative to control virus treatment (figure 3C–F, online supplemental figure 8b-c).

Increased virus replication by oHSV-shPKR could activate both antitumor and antivirus T cell activation. To evaluate if T cell activation was directed against tumor or virus antigens, we used tetramers against EphA2, a known glioma antigen,[22 23] and against virus gB envelop protein. Western blot analysis of infected cells confirmed a significant expression of EphA2 in the infected tumor cell supernatants (online supplemental figure 9) and tetramer analysis of T cells showed a significant increase in percent $EphA2^+$ T cells (figure 3G, online supplemental figure 8d). Interestingly, there was not a significant increase in antivirus gB $tetramer^+$ CTLs (figure 3G, online supplemental figure 8d). The CTLs generated from DCs conditioned with GSC20 cells were evaluated for their ability to kill glioma cells. Increased killing of GSC20 cells but not of unrelated OVTOKO cells by CTLs matured by DCs exposed to oHSV-shPKR treatment (figure 3H). In order to test whether the tumor antigen-specific CTLs had antitumor activity in vivo, GBM12-bearing mice were injected with 2e6 T cells activated by charged DCs, as described in figure 3C. Kaplan-Meier survival curves show that CTLs charged by oHSV-shPKR lysate presenting DCs significantly prolonged animal survival compared with controls (figure 3I). The above results imply that knocking down PKR using an oHSV can suppress antiviral signaling and also improve both antigen presentation to activate CTL activity and tumor-specific activity.

oHSV-PKR regulates tumor immune suppression by controlling TGF-β signaling

To evaluate the impact of oHSV-shPKR on tumor immune environment in vivo, we created an oHSV that encodes for murine PKR targeting shRNA (online supplemental figure 10a). Infection with oHSV-mshPKR efficiently modulated PKR in infected murine GBM cells (online supplemental figure 10b). Treatment of murine glioma (GL261N4) and breast cancer (DB7) cells showed a significant increase in percentage of infected tumor cells and tumor cell death with mu-oHSV-shPKR treatment relative to control oHSV (figure 4A and online supplemental figure 10c–e). To evaluate the effect of modulating PKR by an oHSV in vivo, we treated GL261N4 glioma-bearing mice with mock (saline) or oHSV-shCtl or oHSV-mshPKR, 5 days post tumor cell implant. Three days post treatment (10 days post tumor implant) mice were sacrificed, and single cells isolated from tumor-bearing hemispheres

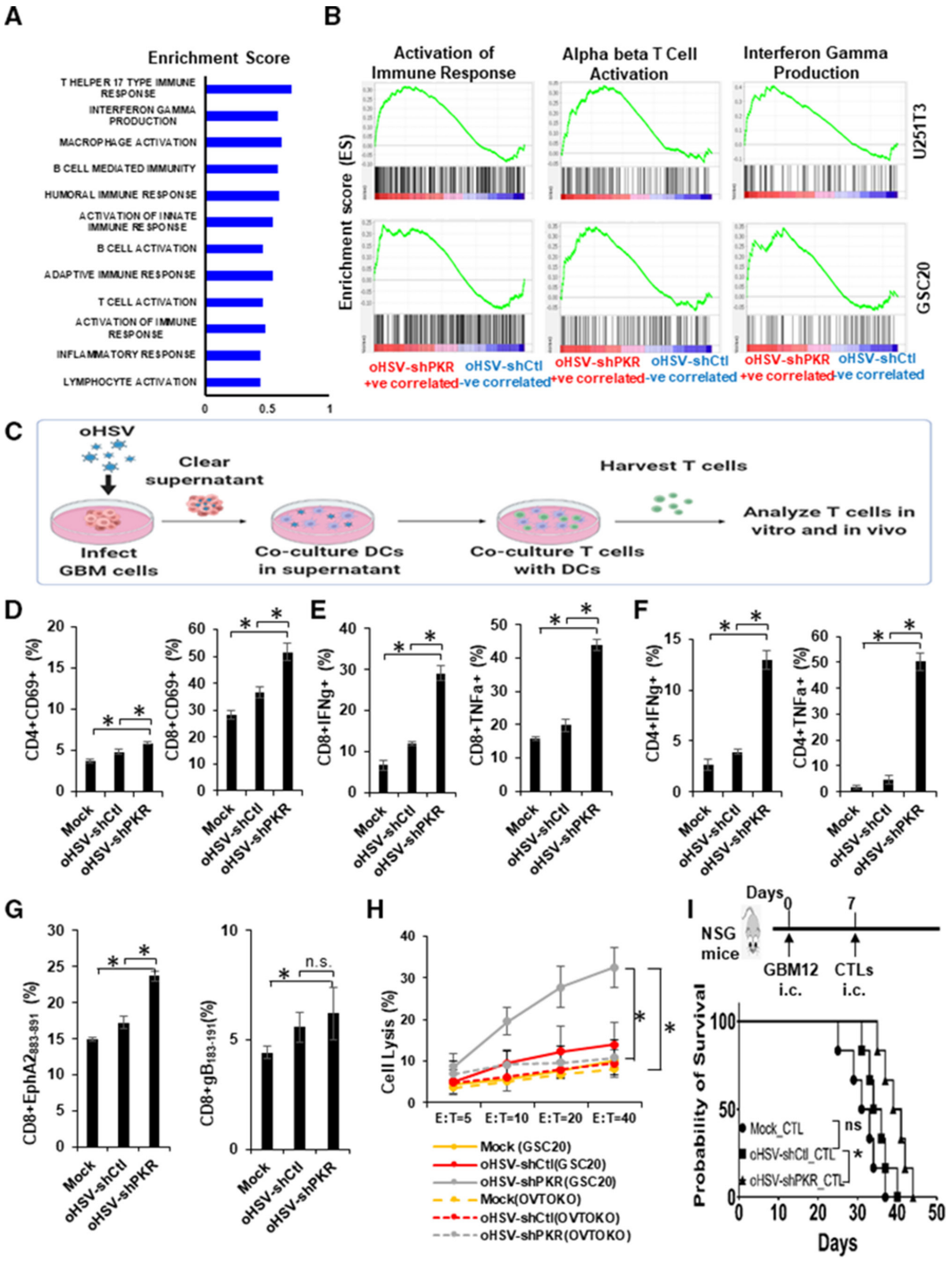

Figure 3 oHSV-shPKR increases antigen-specific cytotoxic T lymphocyte activation. (A) Enriched pathways from mRNA-seq analysis of U251T3 cells infected with oncolytic herpes simplex virus expressing human PKR shRNA (oHSV-shPKR) compared with oHSV-shCtl. (B) Gene set enrichment analysis of U251T3 cells and GSC20 cells infected with oHSV-shPKR compared with oHSV-shCtl for immune response pathways relevant to T cell activation. (C) Experimental scheme used for the analysis of cytotoxic T lymphocyte (CTL) activation by oHSV-shPKR treated glioma cells. (D) Mean±SD % CD69 positive $CD4^+$ and $CD8^+$ T-cells cultured with dendritic cells (n=3/g). (E, F) Mean±SD % of $CD4^+$ and $CD8^+$ T-cells staining positive for intracellular interferon-γ (IFNγ) and tumor necrosis factor alpha (TNFα) (n=3/g). (G) Mean±SD % of CD8 T cells staining positive for anti-glioblastoma (anti-GBM) (EphA2) and antiviral (gB) specificity analyzed by EphA2-tetramer and HSV gB-tetramer staining (n=3/g). (H) The tumor cell lytic activity (mean % lysis±SD) of generated CTLs were tested against $EphA2^+$ GSC20 GBM cells or EphA2- OVTOKO control cancer cells (n=3/g). (I) The antitumor effect of generated CTLs was tested in GBM12-bearing NOD scid gamma (NSG) mice. GBM12-bearing mice were treated with oHSV-shPKR or oHSV-shCtl with or without human T cells and autologous dendritic cells. The survival of tumor-bearing mice was monitored (n=6/group). Data representative of three independent experiments in triplicate. Error bars are SD. One-way analysis of variance followed by Tukey's test for more than two groups. Student's t-test for comparison between two groups. Kaplan-Meier estimator was used to plot survival curve and log-rank test was performed to evaluate the statistical significance (*p value <0.05; n.s., no significance).

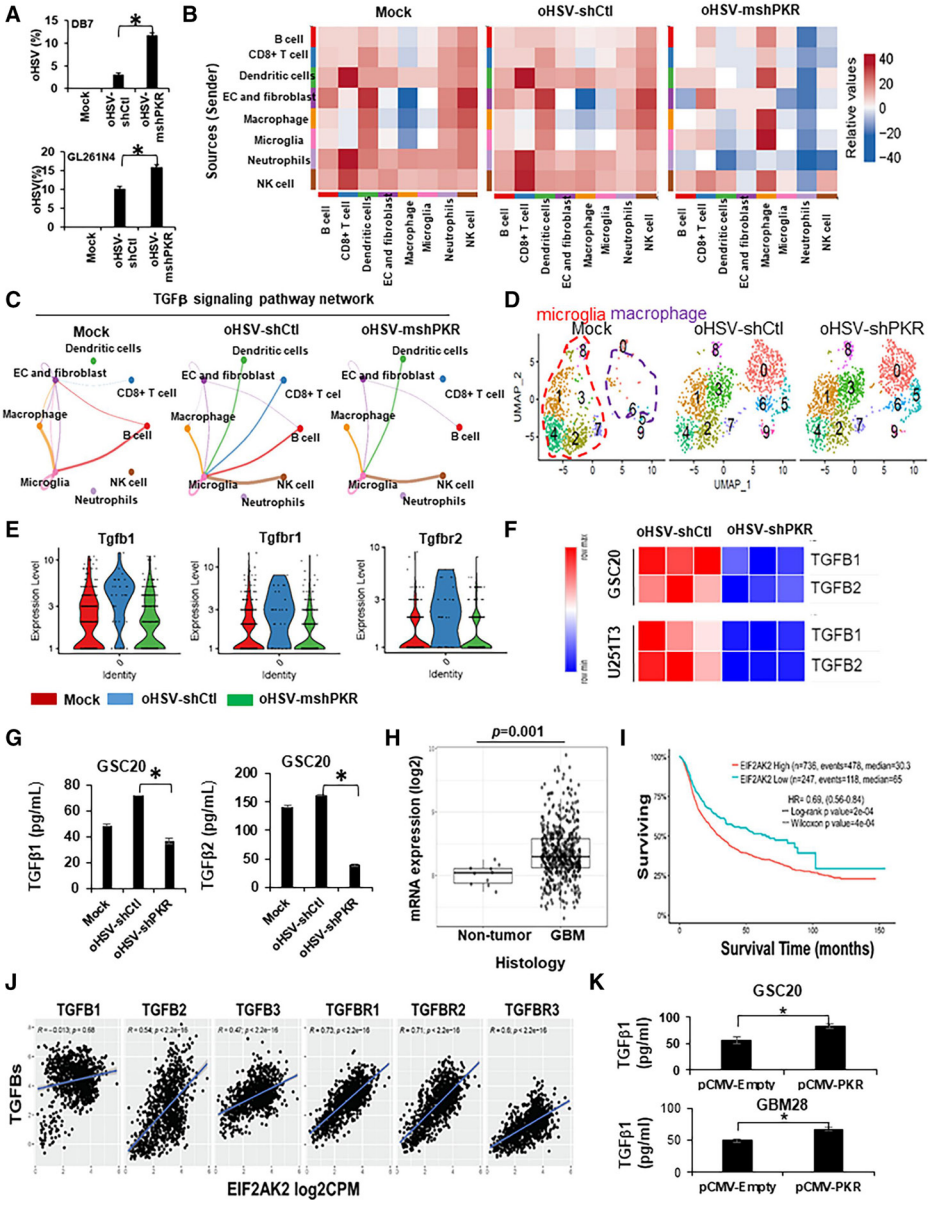

Figure 4 Activated RNA-activated protein kinase (PKR) regulates transforming growth factor beta (TGF-β) signaling. (A) GL261N4 and DB7 cells were infected with oncolytic herpes simplex virus expressing mouse PKR shRNA (oHSV-mshPKR) or oHSV-shCtl (MOI=0.02) for 96 hours. Tumor cell lysis by oHSV-mshPKR in GL261N4 and DB7 cells was analyzed by near-IR live/dead staining (n=3). (B, C) Cell-cell communication analysis using CellChat methods from scRNA-seq data of GL261N4 tumor treated with oHSV-mshPKR or oHSV-shCtl. Murine GL261N4 tumor growing in C57BL/6 mice were treated with oHSV-mshPKR or oHSV-shCtl. Five days after treatment, CD45+ and CD45- cells (1:3 ratio) harvested from tumor-bearing mice were subjected to scRNA-seq analysis (n=5/group). The differential interactions among different immune cell types predicted alterations in oHSV-mshPKR treatment relative to mock-treated and control oHSV-shCtl-treated mice (B). Analysis of net visual aggregate TGF-β signaling pathway quantified from mock, control (oHSV-shCtl) and oHSV-mshPKR-treated animals also showed a reduction in TGF-ß signaling pathway network with oHSV-mshPKR treatment (C). (D) Uniform Manifold Approximation and Projection analysis of myeloid cells of scRNA-seq showed increase macrophages infiltration after oncolytic herpes simplex virus (oHSV) treatment. (E) oHSV-mshPKR treatment significantly downregulates TGF-β signaling in macrophage (cluster 0) relative to oHSV-shCtl treatment. (F) TGF-β heatmap in tumor cells following infection with oHSV-mshPKR or oHSV-shCtl from mRNA-seq analysis. (G) ELISA of TGF-β secretion in tumor cells treated with oHSV-mshPKR or oHSV-shCtl. (H) mRNA expression of PKR in non-tumor versus glioblastoma (GBM) from TCGA dataset including 538 GBM and 10 non-tumor samples. (I) Kaplan-Meier plot using all patients with glioma with overall survival information (n=983) from the Chinese Glioma Genome Atlas (CGGA). Tumors are stratified into two groups with cut-off set as the 25th percentile of the PKR gene expression. (J) Expression correlations between TGF-β-related genes and PKR gene in all patients with glioma (n=6108) from the CGGA. Counts per million are log2-transformed. PKR gene expression is shown as x-axis, while expression of TGF-β-related genes is shown as y-axis. Linear regression line is shown in blue. Wilcoxon rank sum correlation and p values are labeled on top of each scatterplot. (K) TGFβ1 secretion in GBM neurospheres overexpressing PKR was analyzed by ELISA. Experiments were repeated three times with n=3. Error bars are SD, Student's t-test (*p value <0.05).

(CD45+ and CD45-ve (1:3 ratio)) were subjected to single cell sequencing. Cell annotation markers are depicted in online supplemental figure 11. Cell-cell communication analysis to investigate the differential interactions among different immune cell types to predict altered interactions in oHSV-mshPKR treatment relative to mock-treated and control oHSV-shCtl-treated mice was performed using cell chat analysis (figure 4B). oHSV-shPKR treatment altered immune cell interactions with each other relative to mock and oHSV-Ctl treatments. TGF-ß is a key cytokine that mediates Treg differentiation from naïve and effector T cells and is considered a master regulator of antitumor immunity.[24–26] Thus, we evaluated if single cell sequencing of tumors treated with oHSV-mshPKR predicted changes in TGF-β ligand receptor signaling interactions between different cell populations. Analysis of single cell sequencing data for net visual aggregate TGF-β signaling pathway quantified from mock, control (oHSV-shCtl) and oHSV-mshPKR-treated animals also showed a reduction in TGF-ß signaling pathway affecting CD8+ve T cells and microglia with oHSV-mshPKR treatment (figure 4C). Investigation of high-depth single-cell RNA sequencing (RNA-seq) on a cohort of four primary IDH1-negative, grade IV GBMs was analyzed to identify the major cell type within GBM that expresses TGFß1/2/3 and TGFßR1/2/3 revealed that myeloid and vascular cells were the predominant cell types that expressed them.[27] Specifically, TGFβ1 and TGFBR1 and TGFBR2 were highly expressed in myeloid cells (online supplemental figure 12). t-distributed stochastic neighbor embedding (t-SNE) analysis of single cell sequencing data of mice treated with oHSV-shCtl or oHSV-mshPKR showed that both oHSV-shCtl and oHSV-mshPKR treatment increased the infiltration of macrophages (red dotted line) and altered the microglia subpopulation (purple dotted line) relative to untreated tumors. Among these, the cluster 3 (green) in microglia and cluster 0 (red) in macrophages were most highly increased on oHSV-shCtl treatment (figure 4D). Although there was no major difference in the subtypes of macrophage, and microglia, between oHSV-shCtl and oHSV-shPKR-treated groups (figure 4d and online supplemental figure 11b), analysis of changes in TGF-β in these groups uncovered a significant induction of TGFβ1 and TGFβR1, and TGFβR2 in oHSV-shCtl treated tumors in the macrophage subgroup 0 (red) after virotherapy. This induction of TGFβ, TGFβR1 and TGFβR2 was rescued in mice treated with oHSV-mshPKR (figure 4D–E).

mRNA-seq of human glioma cells infected with oHSV-shCtl or oHSV-shPKR also showed a significant reduction in TGF-β gene expression when treated with oHSV-shPKR (figure 4F). Analysis of human glioma cell conditioned medium after treatment with control oHSV-shCtl or oHSVPKR also revealed a significant induction of both TGFβ1 and 2 secretion following treatment with oHSV-shCtl which was significantly rescued by oHSV-shPKR treatment (figure 4G, online supplemental figure 13). GBM are thought to be among the most immune cold tumors and bioinformatic analysis of TCGA database of grade IV patients revealed that PKR is highly expressed in tumor but not non-neoplastic tissue (figure 4H), and patients with a higher PKR expression also correlated with a poor prognosis (figure 4I). To evaluate if TGF-β signaling correlated with PKR in patients with GBM we examined CCGA database, it was revealed that there is a significant correlation between expression levels of PKR and TGFβ1, 2, and 3, and also between PKR and TGFβR1, 2, and 3 (figure 4J). Although we did not see a significant difference in PKR baseline level in oHSV-sensitive and resistant GBM neurospheres (data not shown), however, in vitro overexpression of PKR in GBM neurospheres increased TGF-β secretion (figure 4K).

oHSV-shPKR increases antigen-specific T cell expansion in glioma

Collectively, these results suggest that PKR activation correlates with TGF-β activation and PKR suppression releases TGF-β-induced immune suppression. To evaluate if oHSV-shPKR induced a reactivation of antitumor immunity in the tumor microenvironment in vivo, we used OT-1 transgenic mice, which express T cell receptor that recognizes the 8-mer SINFEKL peptide derived from residues 257–264 of ovalbumin. These OVA expressing tumor cells (GL261N4-OVA) cells are recognized and targeted by OT-1 T-cells. Briefly, GL261N4-OVA cells were infected with either oHSV-mshPKR or control oHSV-shCtl and then co-cultured with splenocytes isolated from OT-I transgenic mice (figure 5A). Representative bright field images revealed increased GL261-OVA cell killing by OT-1 T cells after treatment with oHSV-mshPKR relative to oHSV-shCtl treatment (figure 5A). Quantification of live-dead cell staining by flow cytometry confirmed a significant increase in sensitivity of tumor cells to OT-1 T cells after oHSV-shPKR treatment (figure 5B, online supplemental figure 14a). Analysis of the secretome derived from these co-cultures showed a significant increase in IFNγ and interleukin-2 (IL2) secretion following oHSV-mshPKR-infection compared with control (figure 5C–D). Interestingly, co-culturing splenocytes with either untreated or control virus infected GL261N4-OVA cells significantly suppressed IL2 secretion, but co-culturing with oHSV-mshPKR infected GL261N4-OVA cells significantly increases IL2 production compared with splenocytes alone (figure 5D). Further analysis revealed that infecting GL261N4-OVA cells with oHSV-mshPKR significantly increases the percent $CD8^+$ T cells of total $CD45^+$ splenocytes and also increases the absolute number of $CD8^+$ T-cells in the co-culture (figure 5E–F), indicating expansion in $CD8^+$ T-cells when exposed to oHSV-shPKR-treated tumor cells. Tetramer staining revealed a significant increase in the percentage of OT-1 tetramer staining cells revealed a significant increase in the percent and absolute number of OT-1^+CD8^+ T cells, but again, there was no change in the relative frequency or absolute number of HSV-specific gB^+CD8^+ T cells (figure 5G–H). Phenotypic analysis of the tumor antigen-specific T-cells

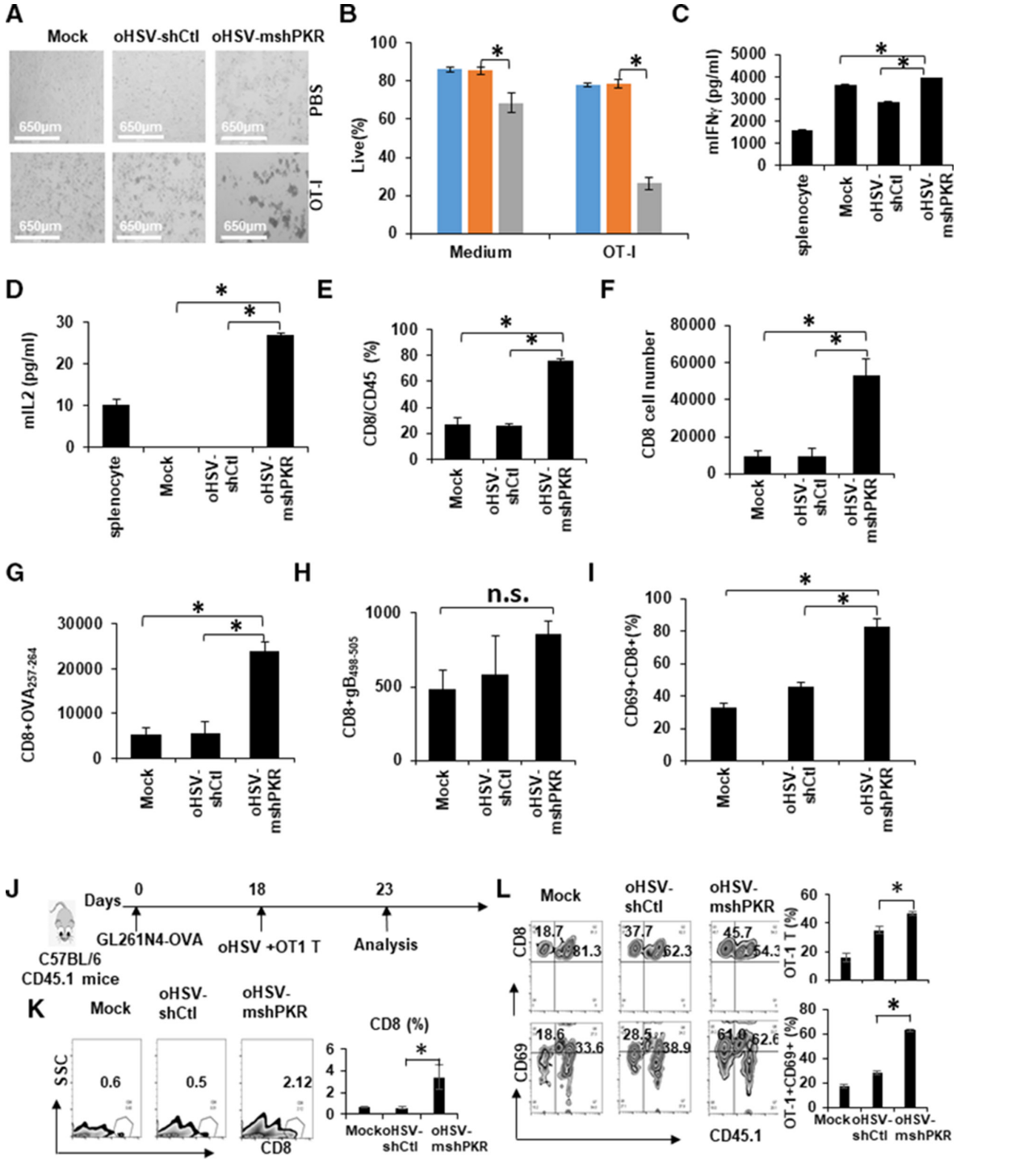

Figure 5 oHSV-mshPKR increases antigen-specific T cell expansion. (A–I) GL261N4-OVA cells were infected with oncolytic herpes simplex virus expressing mouse PKR shRNA (oHSV-mshPKR) or oncolytic herpes simplex virus expressing control shRNA (oHSV-shCtl) with (multiplicity of infection (MOI)=0.05) for 24 hours and then co-cultured with splenocytes from OT-1 transgenic mice (1:5) for 72 hours. Tumor cell lysis by oncolytic herpes simplex virus (oHSV) and OT-I splenocytes was analyzed under bright field microscopy (A) and by flow cytometry analysis of live tumor cells by aqua live/dead staining gating on $CD45^{-ve}$ tumor cells only. Data shown are mean % live±SD. (B)(n=3/g). (C, D) Mean±SD. Interferon γ (IFNγ) and interleukin-2 (IL2) secretion from the co-culture of GL261N4-OVA with OT-I splenocytes was quantified by ELISA assay (n=3/g). $CD8^+$ T cell proliferation and expansion was quantified by flow cytometry of $CD8^+$ and $CD45^+$ populations in the co-culture (E, F) (n=3/g). (G, H) Antigen-specific $CD8^+$ T cell expansion was analyzed by quantifying $OT\text{-}I^{+ve}CD8^{+ve}$ and $HSVgB^{+ve}CD8^{+ve}$ T cells in the co-culture (n=3). (I) $CD8^+$ T cell activation was analyzed by quantifying CD69 expression with flow cytometry (n=3). (J–L) Mouse glioma GL261N4-OVA tumors were established in CD45.1 C57BL/6 mice and treated with $5e^4$ p.f.u. oHSV and OT-1 T cells 18 days later (J). The T cell activation and expansion was evaluated at day 23 (K–L) (n=3). All data are mean of independent triplicate with n=3. Error bars are SD, one-way analysis of variance followed by Tukey's test for more than two groups, Student's t-test for comparison between two groups (*p value <0.05, n.s., no significance).

revealed a significant increase in CD8$^+$ T cells expressing CD69 (figure 5I) and an upregulation of the exhaustion marker PD-1 (online supplemental figure 14b–c). The increase in antigen-specific T cell expansion could also be due in part to more efficient tumor antigen presentation from tumor cells after oHSV-mshPKR infection.[28] Consistent with this, there was increased MHC class I-bound SIINFEKL peptide in GL261N4-OVA after infection with oHSV-mshPKR (online supplemental figure 15).

Our in vitro data show that oHSV-mshPKR is capable of inducing antigen-specific T-cell expansion; therefore, we analyzed the capacity for antigen-specific T-cell expansion and antitumor efficacy following adoptive transfer. GL261N4-OVA tumors were inoculated intracranially into CD45.1$^+$C57BL/6 mice. Tumor-bearing mice were then treated with oHSV-mshPKR or oHSV-shCtl and intratumorally adoptively transferred OT-I$^+$CD8$^+$ T-cells from OT-1 CD45.2-C57BL/6 mice (figure 5J). Five days following adoptive transfer, there was not only a significant increase in the total CD8$^+$ T cell population in the tumor (figure 5K), but also a significant increase in transferred CD45.1$^-$OT-I$^+$CD8$^+$ T-cells in CD45.1 mice treated with oHSV-mshPKR indicating the capacity of these antigen-specific T cells to expand (45.7 vs 37.7) (figure 5L). Furthermore, we found that oHSV-mshPKR treatment significantly increased CD69 expression in both donor (CD45.1$^+$) and recipient (CD45.1$^+$) CD8$^+$ T-cells (figure 5L).

oHSV-mshPKR induces a strong antitumor immune response and antitumor efficacy in vivo

Our results thus far have shown that PKR knockdown in conjunction with oHSV increases antitumor CTL activity; therefore, we next evaluated the impact of oHSV-mshPKR on therapeutic efficacy in immunocompetent syngeneic mouse glioma models. Mice bearing 005 or GL261N4 intracranial brain tumors were treated with virus as indicated and monitored for survival (figure 6A). Kaplan-Meier survival curves demonstrate that intratumoral injection of oHSV-mshPKR significantly inhibited tumor growth and prolonged animal survival in both tumor models analyzed (figure 6A). Immunofluorescence staining of oHSV-mshPKR-treated GL261N4 tumors revealed a reduction in tumor proliferation (Ki-67) and an increase in CD8$^+$ T cell infiltration in oHSV-mshPKR-treated tumors compared with control (figure 6B,C). Flow cytometry and tSNE analysis of tumor infiltrating lymphocytes (TILs) from GL261N4 tumor-bearing mice revealed a significant increase in both effector and memory CD4$^+$ and CD8$^+$ T-cells following oHSV-mshPKR therapy compared with control (figure 6D). The increase of effector CD4 and CD8 T cells in TILs could be due to the inhibition of TGF-β-dependent regulatory T (Treg) cells in the tumor microenvironment. Flow cytometry analysis of TILs showed a significant decrease in CD4+Foxp3+ and CD8+Foxp3 regulatory T cells (figure 6E). In order to detect an antigen-specific antitumor immune response, murine 005 glioma cells expressing the OVA antigen (005-OVA) were established intracranially and treated with oHSV-mshPKR or oHSV-shCtl (figure 6F). Following oHSV therapy, tumors were analyzed for tumor antigen-specific T cells (OVA) and HSV antigen-specific T cells (gB) using tetramer staining. Tumors from mice injected with oHSV-mshPKR had a significant increase in OT-I$^+$CD8$^+$ tumor antigen-specific T cells compared with control, while gB$^+$CD8$^+$ HSV-specific T-cells were significantly increased in oHSV-treated tumors compared with mock, but there was no difference imparted by PKR knockdown (figure 6G,H). Interestingly, we did not detect any significant differences in either the OT-I$^+$CD8$^+$ or the gB$^+$CD8$^+$ T cell populations in the spleen regardless of treatment (figure 6G,H).

Collectively, these results indicate that oHSV-shPKR increases virus-mediated direct tumor cell killing and simultaneously suppresses TGF-ß secretion and signaling thereby inducing antitumor immunity.

DISCUSSION

Mammalian cells have evolved robust pathways to sense and clear intracellular pathogens. The majority of these defense pathways converge on the induction of type 1 interferon signaling which then mobilizes an arsenal of cellular weapons to combat the infectious assault. Among these mechanisms, PKR, a cellular serine threonine kinase, is a key player in the antiviral defense response and serves to orchestrate multiple processes which regulate transcription, translation, apoptosis, and cellular proliferation in the face of a cellular threat. Having a role in several key cellular functions, it is not surprising that the dysregulation of PKR is in turn involved in tumorigenesis, neurodegeneration, inflammation, and metabolic disorders.[29] Specifically, an increased expression of PKR has been correlated with activation of interferon-STAT1 signaling and shown to correspond with a poor prognosis in multiple cancer types. The role for PKR in tumor progression, however, appears to be context dependent: although it is a tumor promoter in some cancer types, in others it functions as a tumor suppressor. For example, PKR has been shown to inhibit the tumor growth of HER2$^+$ breast cancer in mice by affecting cellular proliferation,[30] but in patients with grade IV brain tumor, PKR activation and the ensuing phosphorylation of eIF2α have been shown to be essential for the Musashi-1-driven cancer stem cell-like phenotype and tumor progression.[20] Consistent with the latter, PKR inhibition has been shown to improve the efficiency of anti-cancer vaccines in preclinical mouse models.[31] Here, we show that PKR poses a significant hurdle to the sensitivity of malignant brain tumors to oHSV therapy, and its knockdown results in an increased oncolysis in vitro and in vivo.

PKR-mediated phosphorylation of cellular EIF2α plays a critical role in virus clearance and many viruses have evolved ways to bypass this PKR-mediated phosphorylation and resultant blockade of protein translation. For example, the HSV-1 genome encodes for the viral protein,

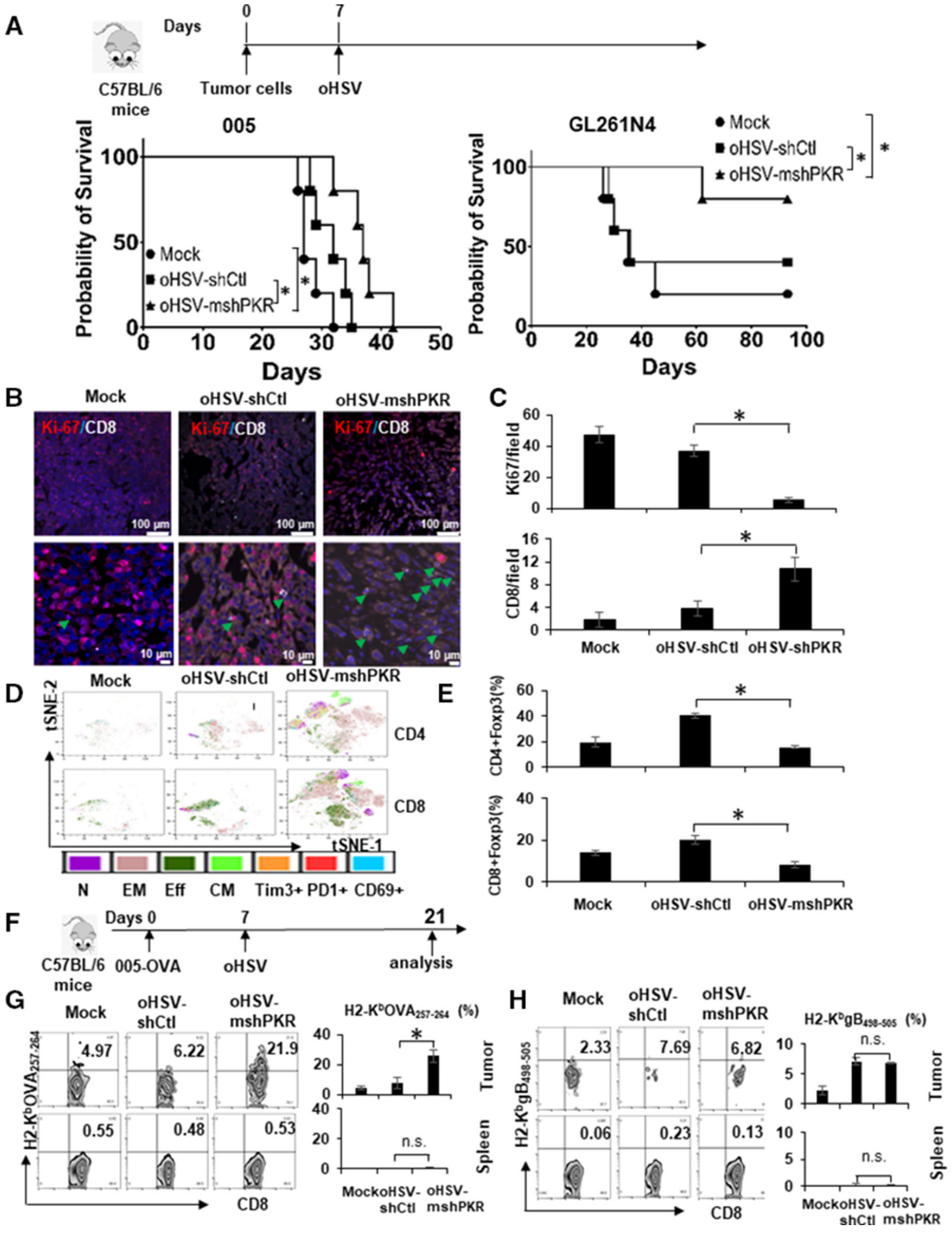

Figure 6 oHSV-mshPKR induces a strong antitumor immune response and antitumor efficacy. (A) Mouse glioma 005 and GL261N4 tumors were established in C57BL/6 mice. Seven days post tumor implant, mice were treated with $5e^4$ p.f.u. oncolytic herpes simplex virus expressing mouse PKR shRNA (oHSV-mshPKR) or oncolytic herpes simplex virus expressing control shRNA (oHSV-shCtl). The survival of tumor-bearing mice was monitored (n=10 mice/group). (B–E) Day 15 of GL261N4 tumor-bearing mice was analyzed for $CD8^+$ T cells and tumor cell proliferation (Ki-67) using immunofluorescence staining. Representative images from one of three mice were shown (B) and quantified (C) (n=7 fields/staining). Green arrows indicate CD8+ve cells. Immune phenotyping of CD4 and CD8 T cells in the tumor-bearing mice was analyzed by flow cytometry and t-distributed stochastic neighbor embedding (tSNE) analysis of pooled CD45+cells from 5 mice (D). CM, central memory T (CD45RA-CCR7+); Eff, effector T (CD45RA+CCR7-); EM, effector memory T (CD45RA-CCR7-); N, Naïve T (CD45RA+CCR7+). Regulatory T cells in treated mice were analyzed by flow cytometry analysis of Foxp3 (n=3) (E). (F–H) Mouse glioma 005-OVA tumors were established in C57BL/6 mice. Seven days later, tumor-bearing mice were treated with $5e^4$ p.f.u. oHSV-mshPKR or oHSV-shCtl. Antitumor and antiviral-specific T cells were analyzed by OT-1-tetramer and HSV gB tetramer staining in tumors and spleens at day 21 post-tumor implantation (G–H) (n=3). Data representative of three independent experiments in triplicate. Error bars are SD, Student's t-test for comparison between two groups and log-rank test for survival curve (*p value <0.05, n.s., no significance). oHSV, oncolytic herpes simplex virus.

ICP34.5, which functions to recruit a cellular phosphatase that dephosphorylates PKR-mediated eIF2α phosphorylation.[32] Apart from ICP34.5, HSV-1 also encodes for US11, which if expressed early in infection cycle can counter PKR activity.[33 34] Apart from inhibiting PKR, ICP34.5 also binds Beclin-1 playing a key role in HSV-1 inhibition through blockade of cellular autophagy.[35] Viruses lacking ICP34.5 are therefore severely attenuated, and indeed almost all HSV-1-derived oncolytic viruses currently being tested in the clinic are deleted for ICP34.5, significantly increasing their safety profiles. Interestingly, it has been recently found that it is more the targeting of Beclin-1 by ICP34.5, rather than the dephosphorylation of eIF2α, that is the major cause of virulence. Indeed, viruses with mutant ICP34.5 that are defective in their ability to bind and inhibit Beclin-1, but intact for reversing PKR-mediated eIF2α phosphorylation, maintain reduced neuro-virulence in vivo.[36 37] Interestingly, early expression of US11 can also counter virus-induced autophagy by a Beclin-1 independent mechanism.[33]

In addition to controlling viral infection, PKR also controls inflammatory signaling and has been implicated in several inflammatory diseases.[38] For example, in the central nervous system (CNS), PKR has been shown to play a direct role in neurodegeneration, as patients diagnosed with either HIV or a neurodegenerative disease such as Alzheimer's, Parkinson's, Huntington's, or dementia have been shown to have increased phosphorylated PKR in their brains.[29] Aside from pathological conditions, the development of stable long-term memory requires de novo protein synthesis, and it has been shown that pharmacologic and genetic approaches to inhibiting PKR improve memory in rodents. Additionally, while PKR activation can induce the release of proinflammatory IL-1β, IL-18, and high mobility group box 1 (HMGB1) proteins, it has also been shown to activate anti-inflammatory IL-10 and reduce $CD8^+$ T cell proliferation in preclinical models.[39] Here, we show that reduction of PKR by an oncolytic virus controls inflammatory antiviral signaling but also promotes DC and T cell-mediated antitumor immunity by rescuing tumor-induced TGF-β secretion.

The TGF-β signaling pathway plays a major role in normal development and its dysregulation is implicated in many diseases, specifically in cancer initiation, progression, and metastasis. TGF-β is highly activated in patients with GBM and is associated with increased invasion and resistance to standard treatments.[40] TGF-β signaling also promotes a shift in cellular metabolism from oxidative phosphorylation to aerobic glycolysis creating a local immunosuppressive microenvironment and encouraging malignant tumor growth.[41] Additionally, TGF-β is considered one of the major pathways by which glioma stem cells induce natural killer (NK) cell dysfunction, resisting immune therapy. Additionally, PKR activation in normal neurons has been attributed to neuron death and memory loss, and mice devoid of PKR are viable and normal,[42 43] thus, we rationalized that an ICP34.5-deleted virus re-engineered to inhibit PKR would retain a safe profile. The finding that PKR induces TGF-β signaling is a very important observation and holds tremendous implications for immunotherapy. However, on the con side PKR activation has also been considered beneficial when combined with cell death inducing agents, possibly via IFN-mediated apoptosis induction.[44] While ablation of PKR in tumor cells has been reported to increase tumorigenicity in some studies, it is important to note that a majority of these studies were conducted in immune-deficient mice.[45]

In this study, we discovered that along with inducing inflammatory responses, PKR significantly induces TGF-β signaling to suppress adaptive immunity, limiting immune-mediated antitumor efficacy. Consistent with these findings, inclusion of a dominant negative PKR in a recent vaccination strategy has been observed to increase the immunogenicity and efficacy of the vaccine.[46] To our knowledge, this is the first report to show the direct regulation of TGF-β production by PKR. Importantly, TGF-β plays a major role in suppressing antitumor immune therapies like immune checkpoint blockade and CAR-T cell therapy.[47] It also has been shown to induce T cell exhaustion.[48] A critical part of the oHSV therapeutic index is activation of antitumor immunity, therefore combining oHSV therapy with immune checkpoint blockade and chimeric antigen receptor (CAR-T) cell therapy is an area of intense investigation.[49–51] Indeed, a recent clinical study combining T-VEC and pembrolizumab found the two agents to have a tolerable profile; however, there was no observable advantage of the combination over pembrolizumab alone. Since mutation in T-VEC facilitate early expression of US11 which can block PKR-mediated eIF2α activation (as opposed to affecting PKR expression like oHSV-shPKR), it will be interesting to evaluate if US11 early expression also affects TGF-β expression.

Gene silencing using siRNA, or shRNA technology could have off-target effects in some circumstances. Although 2–3 siRNA or shRNA targeting both human and mouse PKR are used in this study. Other strategies will be investigated to disable PKR signaling in a tumor-specific manner.

In conclusion, this study uncovered the opposing roles of PKR on innate inflammation and adaptive antitumor immunity in the tumor microenvironment. This makes PKR-mediated virus clearance and suppression of antitumor immunity the Achilles heel of virotherapy, and its destruction improves both oncolysis and antitumor immunity with oHSV. Future studies will evaluate the safety of combining PKR inhibition with oHSV and other immunotherapies for cancer treatment.

MATERIALS AND METHODS

Cells and mice

Patient-derived primary GBM neurospheres GBM12, GBM28, and GSC20 were cultured in 2% fetal bovine serum (FBS) Dulbecco's Modified Eagle Medium

(DMEM) medium. Human GBM cell lines LN229, U87, and U251T3 were cultured in 10% FBS DMEM medium. Murine glioma neurospheres 005, NP, and 005-OVA cell lines were cultured in neurosphere medium supplemented with 100 ng/mL epidermal growth factor (EGF) and fibroblast growth factor (FGF). Murine GL261N4 and GL261N4-OVA cells were cultured in 10% FBS DMEM medium. C57BL/6 (Stock#000664), NOD.*Cg-Prkdc*^{scid}*IL2rg*^{tm1Wjl}/SzJ (NSG, Stock# 005557), C57BL/6-Tg (TcraTcrb)1100Mjb/J (OT-1, Stock#003831), and B6.SJL-*Ptprc*^{a}*Pepc*^{b}/BoyJ (CD45.1, Stock#002014) mice were purchased from Jackson Laboratory. All cells are routinely short tandem repeat (STR) profiled (to validate authenticity and lack of contamination) and are maintained below 30 passages from the last STRS profiling.

Construction of oHSV-shPKR and oHSV-mshPKR

Human oHSV-shPKR was constructed in the laboratory using a modified BAC technology that has been previously described.[52] Human PKR shRNA under the H1 promoter was inserted into HSV-1 genome. A GFP cassette was also inserted into the HSV genome to monitor HSV-infected cells (oHSV-GFP). Recombinant oHSV-shPKR was purified by plaque purification and amplified in Vero cells. Murine oHSV-mshPKR was constructed in a method similar to the human shPKR replaced with murine PKR shRNA. Control oHSV, oHSV-shCtl, was also constructed similar to PKR shRNA replaced with a control scrambled shRNA sequence. All virus preps are tested for purity, contamination and plaque forming ability. Viruses are titrated against a reference control.

Infection, replication, and tumor lysis of oHSV-shPKR in vitro

Infection and replication of oHSV-shPKR and oHSV-mshPKR was assayed in human and murine GBM cells with different MOIs (0.001–0.5) as previously described.[53] Virus-infected GBM cells were quantified as GFP^{+} tumor cells. Tumor cell lysis was quantified by aqua live/dead staining.

Human PBMCs, T cells and PBMC-derived DCs

Human PBMCs were isolated from healthy donors using a buffy coat (Gulf Coast Regional Blood Center, Houston, Texas, USA) by Ficoll gradient centrifugation. T-cells were isolated from PBMCs by negative selection using a T-cell isolation kit (#17951, Stemcell Technologies, California, USA). DCs were derived from PBMCs by culturing with 20 ng/mL hGM-CSF (#300-03, PeproTech, USA) and 20 ng/mL hIL-4 (#200-04, PeproTech) for 7 days.

Co-culturing oHSV-shPKR-infected GBM with immune cells

In order to analyze immune cell-mediated tumor cell lysis, oHSV-shPKR or oHSV-mshPKR infected GBM cells were co-cultured with human PBMCs or murine splenocytes for 3–14 days. Tumor cell lysis and immune cell phenotype were analyzed using flow cytometry.

In vivo human GBM PDX xenograft models and murine GBM models

The antitumor efficacy of oHSV-shPKR was tested in human GBM PDX models in immune-deficient NOD scid gamma (NSG) mice. GBM12, GSC20, or U87 cells were inoculated intracranially into NSG mice aged 5–6 weeks old. Tumor-bearing mice were then intratumorally injected with oHSV-shCtl or oHSV-shPKR. CTLs generated in vitro were injected into tumor-bearing mice to test tumor lysis efficacy.

The antitumor efficacy of oHSV-mshPKR was tested in syngeneic mouse GBM models. GL261N4, 005, GL261N4-OVA, and 005-OVA were intracranially inoculated into C57BL/6 or CD45.1 mice. Tumor-bearing mice were treated with oHSV-mshPKR or oHSV-shCtl with or without antigen-specific T-cell transfer (OT-1 cells). Antitumor immune response was monitored by OT-1 and HSVgB tetramer staining and immune cell profiling.

Flow cytometry

For cell surface staining, cells were washed with phosphate-buffed saline (PBS) and blocked with Fc blocker (BD Biosciences, San Jose, California, USA). Fluorochrome-labeled antibodies (Annexin-V, CD45, CD11c, CD4, CD8, CD11b, Ly6G, Ly6C, PD-1, PD-L1, F4/80, CD56, CD86, HLA-DR, CD206, and CD44) were obtained from BD Biosciences (Franklin Lakes, USA), added, and stained for 30 min as described.[54] For intracellular staining, cells were permeabilized with Fix/Perm buffer (#FC009, R&D Systems, Minneapolis, Minnesota, USA) for 20 min and then washed with Perm/Wash buffer (R&D Systems). Fluorochrome-labeled antibodies (IFNγ and TNFα) (#562019, #561062, BD Biosciences) were diluted in Perm/wash buffer and stained for 30 min as described.[55] All samples were analyzed on a CytoFlex flow cytometer (Beckman Coulter, California, USA).

Tetramer staining

Antigen-specific CD8^{+} T cells in human or murine tumors were analyzed by tetramer staining. H-2K^{b}-restricted OVA ($OVA_{257-264}$) or HSV glycoprotein B ($gB_{498-505}$) tetramers were purchased from the NCI tetramer facility. HLA*A2:0201-restricted $EphA2_{883-891}$[23 26] or HSV glycoprotein B ($gB_{183-191}$)[56] tetramers were ordered from the tetramer facility at Baylor College of Medicine. Human CD8^{+} T cells were stained with $EphA2_{883-891}$ or HSV $gB_{183-191}$ tetramer and CD8 for 30 min. Murine CD8^{+} T cells were stained with $OVA_{257-264}$ or HSV $gB_{498-505}$ tetramer and CD8 for 30 min. Cells were then washed with PBS and analyzed using CytoFlex (Beckman Coulter).

Western blot

Whole cell lysates were prepared and loaded onto sodium dodecyl sulfate-polyacrylamide gel electrophoresis (SDS-PAGE). After transfer, the membrane was blocked with 5% skim milk in Tris-buffered saline (TBS) supplemented with 0.05% Tween 20 (TBST) for 1 hour and then incubated in diluted primary antibodies PKR, p90RSK, tubulin

(#ab210797) or GAPDH (#ab181602) (obtained from Abcam, Cambridge, USA) overnight. The membrane was washed with TBS-T three times and incubated with an horseradish peroxidase (HRP)-labeled secondary antibody for 1 hour. The membrane was developed using a Bio-Rad developer system.

RNA library construction and data analysis

For RNA sequencing (RNA-seq), total RNA was prepared from GSC20 and U251T3 cells treated with oHSV-shPKR or oHSV-shCtl (MOI=0.02) for 72 hours. Total RNA was extracted using a RNeasy mini-kit (#74104, Qiagen, Germany). Poly (A)-tailed messenger RNA was enriched and the RNA-seq library was constructed following the manufacturer's instructions for the KAPA mRNA HyperPrep Kit (#KK8581, Roche Holding AG, Switzerland) and the KAPA Unique Dual-indexed Adapter kit (KK8727, Roche Holding AG) by the UTHealth Cancer Genomics Core. RNA-seq data were generated by an Illumina Nextseq 550 using the 75 bp pair-ended running mode.

Raw mRNA sequence reads were preprocessed using Cutadapt (V.1.15) to remove bases with quality scores <20 and adapter sequences.[57] Clean RNA-seq reads were aligned to the reference genome GRCh38.102 using STAR (V.2.5.3a).[58] Gene abundance was quantified and normalized by Transcripts Per Million (TPM) using RSEM (V.1.3.0).[59] GSEA was conducted using RDAVID WebService (V.1.19.0)[60] for Gene Ontology (GO) terms and R package for pathway analysis. The enrichment p values were adjusted by following the Benjamini and Hochberg's approach.[61]

Single-cell data analysis

Single-cell RNA sequencing (scRNA-seq) were performed from GL261N4 tumor treated with oHSV-mshPKR or oHSV-shCtl in vivo. Murine GL261N4 tumor growing in C57BL/6 mice were treated with oHSV-mshPKR or oHSV-shCtl. Five days after treatment, CD45+ and CD45- cells (1:3 ratio) harvested from tumor-bearing mice were subjected to scRNA-seq analysis (n=5/group). The demultiplexed clean reads were aligned against the UCSC mouse GRCm38 reference genome by cell ranger. After constructing the single-cell gene expression count matrix, we used the R package Seurat (V.4.0)[62] for downstream analysis on the R platform (V.4.1.2). Cells with transcriptional noise were first filtered using several criteria, including minimal expression of 200 genes per cell and mitochondrial read percentages >10%. All cells passing quality control were merged into one count matrix and normalized and scaled using Seurat's NormalizeData and ScaleData functions. The reduced set of consensus highly variable genes was used as the feature set for independent component analysis using Seurat's RunPCA function. A Uniform Manifold Approximation and Projection (UMAP) dimensional reduction analysis was performed on the scaled matrix (with only the most variable genes) using the first 30 principal component analysis (PCA) components to obtain a two-dimensional representation of the cell states. Cell clusters were identified using the shared nearest neighbor algorithm with a resolution parameter of 0.6. The differentially expressed genes (DEGs) analysis between different cell clusters was conducted by Wilcoxon rank-sum test implemented in the Seurat 'FindAllMarkers' function. For each cluster, only the genes that were expressed in >25% of cells with at least a 0.25-fold difference were considered marker genes. To aid in the assignment of cell type to clusters derived from unsupervised clustering, we performed cell-type enrichment analysis based on deCS package, using cluster-specific genes.[56] Mouse gene symbols were capitalized to map to human gene symbols.

Cell-cell communication analysis

oHSV delivery of PKR knockdown in brain tumor cells may affect brain immune cellular interactions through an interactive connection among immune cell types, including antigen presentation cells, effector T cells, B cells and myeloid cells, including macrophage, microglia, neutrophils and other non-immune cells including endothelial cells and fibroblast.[63] To identify and visualize the immune cell state-specific cell-cell interactions, we employed an R package called CellChat[64] to infer cell-to-cell interactions in oHSV-mshPKR treatment or oHSV-shCtl or mock treatment. Briefly, we loaded the normalized counts into CellChat and applied the standard preprocessing steps, which involved the application of the functions *identifyOverExpressedGenes*, *identifyOverExpressedInteractions*, and *projectData* with default parameter settings. Prevalidated ligand-receptor (L-R) interactions were selectively used as a priori network information. For each L-R pair, we then calculated their information flow strength and communication probability between different cell groups by using the functions *computeCommunProb*, *computeCommunProbPathway*, and *aggregateNet* with standard parameters.[64] Together, the overall communication probabilities among all pairs of cell groups across all pairs of L-R interactions were transformed into a three-dimensional tensor P ($K \times K \times N$), where K corresponds to six cell groups and N corresponds to L-R pairs of different signaling pathways.[64]

To predict significant intercellular communications between the oHSV-mshPKR and oHSV-shPKR or mock treatment, for each L-R pair, we used a one-sided permutation test (n=100), which randomly permuted the group labels of cells and then recalculated the communication probability between two cell groups.[64] The interactions with a p value <0.05 were considered statistically significant.

Statistical analysis

All quantitative results are displayed as mean±SD. The statistical difference between two groups was compared using a Mann-Whitney U test or a Student's t-test. If more than two groups were compared, analysis of variance was used. Statistical analysis was determined using Prism V.5

software (GraphPad Software, La Jolla, California, USA). A p value <0.05 was considered statistically significant.

Contributors BH and BK conceptualized and designed the studies. BH, US, MPM, EH, YO and YS performed the experiments. BH, US, MPM, EH, JY, MAC, and BK analyzed the data. GP, YY, HF, and ZZ performed statistical and RNA sequencing analysis. BH and BK wrote the manuscript. Guarantors: BH and BK. All authors edited and reviewed the manuscript.

Funding This study was supported by grants from NIH/NCI P01CA163205 (to BK), NIH/NINDS R61NS112410 (to BK), and the Cancer Prevention and Research Institute of Texas (CPRIT RP180734 to ZZ, RP210045 to ZZ and BK).

Competing interests None declared.

Patient consent for publication Not applicable.

Ethics approval Not applicable.

Provenance and peer review Not commissioned; externally peer reviewed.

Data availability statement Data are available upon reasonable request.

ORCID iDs
Zhongming Zhao http://orcid.org/0000-0002-3477-0914
Balveen Kaur http://orcid.org/0000-0001-7738-0804

REFERENCES

1 Cassady KA, Gross M. The herpes simplex virus type 1 U(S)11 protein interacts with protein kinase R in infected cells and requires a 30-amino-acid sequence adjacent to a kinase substrate domain. *J Virol* 2002;76:2029–35.
2 Elde NC, Child SJ, Geballe AP, *et al*. Protein kinase R reveals an evolutionary model for defeating viral mimicry. *Nature* 2009;457:485–9.
3 Pindel A, Sadler A. The role of protein kinase R in the interferon response. *J Interferon Cytokine Res* 2011;31:59–70.
4 Hu M-M, Yang Q, Xie X-Q, *et al*. Sumoylation promotes the stability of the DNA sensor cgas and the adaptor sting to regulate the kinetics of response to DNA virus. *Immunity* 2016;45:555–69.
5 Ishikawa H, Ma Z, Barber GN. Sting regulates intracellular DNA-mediated, type I interferon-dependent innate immunity. *Nature* 2009;461:788–92.
6 Reinert LS, Lopušná K, Winther H, *et al*. Sensing of HSV-1 by the cgas-STING pathway in microglia orchestrates antiviral defence in the CNS. *Nat Commun* 2016;7:13348.
7 Reinert LS, Rashidi AS, Tran DN, *et al*. Brain immune cells undergo cgas/STING-dependent apoptosis during herpes simplex virus type 1 infection to limit type I IFN production. *J Clin Invest* 2021;131:e136824.
8 Hou B, Saudan P, Ott G, *et al*. Selective utilization of Toll-like receptor and MyD88 signaling in B cells for enhancement of the antiviral germinal center response. *Immunity* 2011;34:375–84.
9 Liu H, Chen K, Feng W, *et al*. TLR4-myd88/mal-NF-kb axis is involved in infection of HSV-2 in human cervical epithelial cells. *PLoS One* 2013;8:e80327.
10 Critchley-Thorne RJ, Simons DL, Yan N, *et al*. Impaired interferon signaling is a common immune defect in human cancer. *Proc Natl Acad Sci U S A* 2009;106:9010–5.
11 Kaufman HL, Maciorowski D. Advancing oncolytic virus therapy by understanding the biology. *Nat Rev Clin Oncol* 2021;18:197–8.
12 Kurokawa C, Iankov ID, Anderson SK, *et al*. Constitutive interferon pathway activation in tumors as an efficacy determinant following oncolytic virotherapy. *J Natl Cancer Inst* 2018;110:1123–32.
13 Hou W, Sampath P, Rojas JJ, *et al*. Oncolytic virus-mediated targeting of PGE2 in the tumor alters the immune status and sensitizes established and resistant tumors to immunotherapy. *Cancer Cell* 2016;30:108–19.
14 Bommareddy PK, Aspromonte S, Zloza A, *et al*. Mek inhibition enhances oncolytic virus immunotherapy through increased tumor cell killing and T cell activation. *Sci Transl Med* 2018;10:eaau0417.
15 Uche IK, Kousoulas KG, Rider PJF. The effect of herpes simplex virus-type-1 (HSV-1) oncolytic immunotherapy on the tumor microenvironment. *Viruses* 2021;13:1200.
16 Vähä-Koskela MJV, Le Boeuf F, Lemay C, *et al*. Resistance to two heterologous neurotropic oncolytic viruses, Semliki Forest virus and vaccinia virus, in experimental glioma. *J Virol* 2013;87:2363–6.
17 Mineta T, Rabkin SD, Yazaki T, *et al*. Attenuated multi-mutated herpes simplex virus-1 for the treatment of malignant gliomas. *Nat Med* 1995;1:938–43.
18 Muik A, Stubbert LJ, Jahedi RZ, *et al*. Re-Engineering vesicular stomatitis virus to abrogate neurotoxicity, circumvent humoral immunity, and enhance oncolytic potency. *Cancer Res* 2014;74:3567–78.
19 Shir A, Levitzki A. Inhibition of glioma growth by tumor-specific activation of double-stranded RNA-dependent protein kinase PKR. *Nat Biotechnol* 2002;20:895–900.
20 Chen H-Y, Lin L-T, Wang M-L, *et al*. Musashi-1 promotes chemoresistant granule formation by PKR/eif2α signalling cascade in refractory glioblastoma. *Biochim Biophys Acta Mol Basis Dis* 2018;1864(5 Pt A):1850–61.
21 Feng Z-Z, Luo N, Liu Y, *et al*. Er stress and its PERK branch enhance TCR-induced activation in regulatory T cells. *Biochem Biophys Res Commun* 2021;563:8–14.
22 Binda E, Visioli A, Giani F, *et al*. The epha2 receptor drives self-renewal and tumorigenicity in stem-like tumor-propagating cells from human glioblastomas. *Cancer Cell* 2012;22:765–80.
23 Hatano M, Eguchi J, Tatsumi T, *et al*. Epha2 as a glioma-associated antigen: a novel target for glioma vaccines. *Neoplasia* 2005;7:717–22.
24 Chen W, Jin W, Hardegen N, *et al*. Conversion of peripheral CD4+CD25- naive T cells to CD4+CD25+ regulatory T cells by TGF-beta induction of transcription factor FOXP3. *J Exp Med* 2003;198:1875–86.
25 Marie JC, Letterio JJ, Gavin M, *et al*. Tgf-Beta1 maintains suppressor function and FOXP3 expression in CD4+CD25+ regulatory T cells. *J Exp Med* 2005;201:1061–7.
26 Wan YY, Flavell RA. " Yin-Yang " functions of transforming growth factor-beta and T regulatory cells in immune regulation. *Immunol Rev* 2007;220:199–213.
27 Darmanis S, Sloan SA, Croote D, *et al*. Single-cell RNA-seq analysis of infiltrating neoplastic cells at the migrating front of human glioblastoma. *Cell Rep* 2017;21:1399–410.
28 Goel S, DeCristo MJ, Watt AC, *et al*. Cdk4/6 inhibition triggers anti-tumour immunity. *Nature* 2017;548:471–5.
29 Gal-Ben-Ari S, Barrera I, Ehrlich M, *et al*. Pkr: a kinase to remember. *Front Mol Neurosci* 2018;11:480.
30 Darini C, Ghaddar N, Chabot C, *et al*. An integrated stress response via PKR suppresses HER2+ cancers and improves trastuzumab therapy. *Nat Commun* 2019;10:2139.
31 Zhang W, Liu Y, Min Chin J, *et al*. Sustained release of PKR inhibitor C16 from mesoporous silica nanoparticles significantly enhances mrna translation and anti-tumor vaccination. *Eur J Pharm Biopharm* 2021;163:179–87.
32 Hong B, Sahu U, Mullarkey MP, *et al*. Replication and spread of oncolytic herpes simplex virus in solid tumors. *Viruses* 2022;14:118.
33 Lussignol M, Queval C, Bernet-Camard M-F, *et al*. The herpes simplex virus 1 US11 protein inhibits autophagy through its interaction with the protein kinase PKR. *J Virol* 2013;87:859–71.
34 Liu BL, Robinson M, Han Z-Q, *et al*. Icp34.5 deleted herpes simplex virus with enhanced oncolytic, immune stimulating, and anti-tumour properties. *Gene Ther* 2003;10:292–303.
35 A M, A A, E A, *et al*. The propagation of HSV-1 in high autophagic activity. *Microb Pathog* 2021;152:104599.
36 Orvedahl A, Alexander D, Tallóczy Z, *et al*. Hsv-1 ICP34.5 confers neurovirulence by targeting the Beclin 1 autophagy protein. *Cell Host Microbe* 2007;1:23–35.
37 Leib DA, Alexander DE, Cox D, *et al*. Interaction of ICP34.5 with Beclin 1 modulates herpes simplex virus type 1 pathogenesis through control of CD4+ T-cell responses. *J Virol* 2009;83:12164–71.
38 Kang R, Tang D. Pkr-Dependent inflammatory signals. *Sci Signal* 2012;5:pe47.

39 Chakrabarti A, Sadler AJ, Kar N, *et al*. Protein kinase R-dependent regulation of interleukin-10 in response to double-stranded RNA. *J Biol Chem* 2008;283:25132–9.
40 Joseph JV, Magaut CR, Storevik S, *et al*. TGF-β promotes microtube formation in glioblastoma through thrombospondin 1. *Neuro Oncol* 2022;24:541–53.
41 Gong L, Ji L, Xu D, *et al*. Tgf-B links glycolysis and immunosuppression in glioblastoma. *Histol Histopathol* 2021;36:1111–24.
42 Couturier J, Morel M, Pontcharraud R, *et al*. Interaction of double-stranded RNA-dependent protein kinase (PKR) with the death receptor signaling pathway in amyloid beta (Abeta) -treated cells and in APPSLPS1 knock-in mice. *J Biol Chem* 2010;285:1272–82.
43 Yang YL, Reis LF, Pavlovic J, *et al*. Deficient signaling in mice devoid of double-stranded RNA-dependent protein kinase. *EMBO J* 1995;14:6095–106.
44 Marchal JA, Carrasco E, Ramirez A, *et al*. Bozepinib, a novel small antitumor agent, induces PKR-mediated apoptosis and synergizes with IFNα triggering apoptosis, autophagy and senescence. *Drug Des Devel Ther* 2013;7:1301–13.
45 Yoon CH, Lee ES, Lim DS, *et al*. Pkr, a p53 target gene, plays a crucial role in the tumor-suppressor function of p53. *Proc Natl Acad Sci U S A* 2009;106:7852–7.
46 Lihoradova O, Kalveram B, Indran SV, *et al*. The dominant-negative inhibition of double-stranded RNA-dependent protein kinase PKR increases the efficacy of Rift Valley fever virus MP-12 vaccine. *J Virol* 2012;86:7650–61.
47 Caruana I, Savoldo B, Hoyos V, *et al*. Heparanase promotes tumor infiltration and antitumor activity of CAR-redirected T lymphocytes. *Nat Med* 2015;21:524–9.
48 Weber EW, Parker KR, Sotillo E, *et al*. Transient rest restores functionality in exhausted CAR-T cells through epigenetic remodeling. *Science* 2021;372:eaba1786.
49 Brudno JN, Lam N, Vanasse D, *et al*. Safety and feasibility of anti-CD19 CAR T cells with fully human binding domains in patients with B-cell lymphoma. *Nat Med* 2020;26:270–80.
50 Chen J, López-Moyado IF, Seo H, *et al*. Nr4A transcription factors limit CAR T cell function in solid tumours. *Nature* 2019;567:530–4.
51 Ghosh A, Smith M, James SE, *et al*. Donor CD19 CAR T cells exert potent graft-versus-lymphoma activity with diminished graft-versus-host activity. *Nat Med* 2017;23:242–9.
52 Kuroda T, Martuza RL, Todo T, *et al*. Flip-Flop HSV-BAC: bacterial artificial chromosome based system for rapid generation of recombinant herpes simplex virus vectors using two independent site-specific recombinases. *BMC Biotechnol* 2006;6:40.
53 Direnzo GJ. Dogmatism and presidential preferences: a 1968 replication. *Psychol Rep* 1971;29:109–10.
54 Hong B, Chapa V, Saini U, *et al*. Oncolytic HSV therapy modulates vesicular trafficking inducing cisplatin sensitivity and antitumor immunity. *Clin Cancer Res* 2021;27:542–53.
55 Russell L, Swanner J, Jaime-Ramirez AC, *et al*. Pten expression by an oncolytic herpesvirus directs T-cell mediated tumor clearance. *Nat Commun* 2018;9:5006.
56 Khan AA, Srivastava R, Spencer D, *et al*. Phenotypic and functional characterization of herpes simplex virus glycoprotein B epitope-specific effector and memory CD8+ T cells from symptomatic and asymptomatic individuals with ocular herpes. *J Virol* 2015;89:3776–92.
57 Martin M. Cutadapt removes adapter sequences from high-throughput sequencing reads. *EMBnet j* 2011;17:10.
58 Dobin A, Davis CA, Schlesinger F, *et al*. Star: ultrafast universal RNA-seq aligner. *Bioinformatics* 2013;29:15–21.
59 Li B, Dewey CN. RSEM: accurate transcript quantification from RNA-Seq data with or without a reference genome. *BMC Bioinformatics* 2011;12:323.
60 Fresno C, Fernández EA. RDAVIDWebService: a versatile R interface to David. *Bioinformatics* 2013;29:2810–1.
61 Benjamini Y, Hochberg Y. Controlling the false discovery rate: a practical and powerful approach to multiple testing. *J R Stat Soc: Series B (Methodological)* 1995;57:289–300.
62 Butler A, Hoffman P, Smibert P, *et al*. Integrating single-cell transcriptomic data across different conditions, technologies, and species. *Nat Biotechnol* 2018;36:411–20.
63 Yeo AT, Rawal S, Delcuze B, *et al*. Single-Cell RNA sequencing reveals evolution of immune landscape during glioblastoma progression. *Nat Immunol* 2022;23:971–84.
64 Jin S, Guerrero-Juarez CF, Zhang L, *et al*. Inference and analysis of cell-cell communication using cellchat. *Nat Commun* 2021;12:1088.